Characterizing High-Voltage Neighborhood with Unique AC Power Flow Solution

Jiawei Zhao, Minghua Chen, *Fellow, IEEE*, and Steven H. Low, *Fellow, IEEE*

***Abstract*—The AC power flow (PF) problem determines steady-state grid voltages from nonlinear equations that may admit multiple solutions. Among them, high-voltage (HV) solutions, whose bus-voltage magnitudes lie within normal operating ranges, are of primary operational interest. Given a reference HV operating point, we seek the largest centered hyperrectangle with a prescribed aspect ratio over which the PF mapping is injective, ensuring a unique PF solution within the region. Exploiting the quadratic structure of the PF equations in Cartesian coordinates, we show that this problem is equivalent to solving a collection of nonconvex quadratically constrained quadratic programs (QCQPs) whose number grows linearly with network size. To our knowledge, this is the first exact characterization of such a unique-solution neighborhood. To address the nonconvexity of the QCQPs, we compute an inner approximation using semidefinite programming and quadratic-convex relaxations and an outer approximation using an interior-point method. We further develop a method for provably combining multiple certified HV neighborhoods into a larger, potentially nonconvex region while preserving injectivity. Simulations on IEEE test systems show that the proposed method identifies unique-solution neighborhoods up to two orders of magnitude larger than those obtained by state-of-the-art methods, covering voltage ranges comparable to normal operating ranges.**

***Index Terms*—Power flow equations, high-voltage power flow solution, quadratic mapping, quadratically constrained quadratic programming (QCQP), convex relaxation**

NOMENCLATURE

$\mathcal{N}$	Set of buses, $N \triangleq \text{card}(\mathcal{N})$.
$\mathcal{G}$	Set of PV buses.
$\mathcal{D}$	Set of PQ buses.
P_i	Active power injection at bus i.
Q_i	Reactive power injection at bus i.
V_i	Complex voltage at bus i, where $V_i = e_i + \mathrm{j} f_i$.
e_i, f_i	Real and imaginary components of V_i.
$\mathbf{e}$, $\mathbf{f}$	Real and imaginary voltage vectors for all buses, where $\mathbf{e} = [e_i,\, i \in \mathcal{N}]^\top$ and $\mathbf{f} = [f_i,\, i \in \mathcal{N}]^\top$.
$\tilde{\mathbf{e}}$, $\tilde{\mathbf{f}}$	Real and imaginary voltage vectors for non-slack buses, where $\tilde{\mathbf{e}} = [e_i,\, i \in \mathcal{D} \cup \mathcal{G}]^\top$ and $\tilde{\mathbf{f}} = [f_i,\, i \in \mathcal{D} \cup \mathcal{G}]^\top$.
$\mathbf{e}_0$, $\mathbf{f}_0$	Reference real and imaginary voltage vectors for non-slack buses, where $\mathbf{e}_0 = [e_{0,i}, i \in \mathcal{D} \cup \mathcal{G}]^\top$ and $\mathbf{f}_0 = [f_{0,i}, i \in \mathcal{D} \cup \mathcal{G}]^\top$.
Y	Admittance matrix, where $Y_{ij} = G_{ij} + \mathrm{j} B_{ij}$.
$\|\mathbf{t}\|_p$	ℓ_p-norm of vector $\mathbf{t}$; $\|\mathbf{t}\|_\infty = \max_i \|t_i\|$ denotes the ℓ_∞-norm.

I. INTRODUCTION

The power flow (PF) problem determines bus-voltage magnitudes and angles from specified load demands, generator outputs, and generator-bus voltage setpoints. It underpins applications including system planning [1], [2], contingency analysis [3], and steady-state security assessment [4], where it identifies branch overloads and bus-voltage limit violations.

Owing to their nonlinearity, the PF equations may admit multiple solutions, up to 2^{N-1} for an N-bus system [5]. Among these mathematically valid solutions, high-voltage (HV) solutions, whose voltages lie within normal operating ranges, are most relevant to routine operation. If the same specified operating condition admits multiple HV solutions, a PF solver may converge to one that does not represent the realized operating point, potentially distorting security assessments and subsequent operational decisions.

Characterizing regions with unique PF solutions is therefore of great interest. Accordingly, we study the following question: *given an HV operating point, how to characterize the largest neighborhood over which the PF mapping is injective and hence the PF solution is unique*?

Existing studies approach this question primarily by deriving sufficient conditions that certify uniqueness over prescribed regions. For distribution networks, fixed-point methods establish explicit uniqueness conditions based on loading and network parameters [6]–[9]. For P-θ networks comprising only PV buses, graph-theoretic methods define uniqueness regions through bounds on phase-angle differences [10]–[12]. For general transmission networks, monotone-operator methods construct convex voltage domains in which the PF equations admit at most one solution [13]. Other studies combine topological degree theory with the implicit function theorem to estimate unique-solution neighborhoods around a given solution [14], [15]. However, these approaches do not generally characterize the largest unique-solution neighborhood: they either require restrictive network assumptions or produce conservative estimates, covering less than 1% of the normal voltage operating range [15], [16]. See more discussions on related work in Section II.

In this paper, we develop an approach for characterizing largest unique-solution neighborhoods around an HV operating

This work is supported in part by a General Research Fund from Research Grants Council, Hong Kong (Project No. 11200124), a Collaborative Research Fund from Research Grants Council, Hong Kong (Project No. C1049-24G), and a Start-up Research Grant from The Chinese University of Hong Kong, Shenzhen (Project No. UDF01004086); and in part by the Caltech Resnick Sustainability Institute and the S2I grants.

J. Zhao is with Department of Data Science, City University of Hong Kong. M. Chen is with School of Data Science, The Chinese University of Hong Kong, Shenzhen, on leave from Department of Data Science, City University of Hong Kong. S. Low is with Computing and Mathematical Sciences and Electrical Engineering, Caltech. Corresponding author: M. Chen.

TABLE I
COMPARISON OF EXISTING STUDIES ON POWER FLOW SOLUTION EXISTENCE AND UNIQUENESS.

Network Type	Existing Study	Existence	Solvable Input Region		Uniqueness	HV Solution Neighborhood		Method
			Inner Bound	Outer Bound		Inner Bound	Outer Bound	
Distribution	[6]–[9]	✓	Tight	N.A.	✓	Tight	N.A.	Fixed-point theorem
	[17]	✓	Tight	N.A.	✓	N.A.	N.A.	Energy function; fixed-point
P-θ	[10], [11]	×	N.A.	N.A.	✓	Tight	Tight	Graph theory
	[12]	✓	Tight	N.A.	✓	Tight	N.A.	Cycle-space analysis
General	[18]	✓	N.A.	Tight	×	N.A.	N.A.	Semidefinite programming
	[19]	✓	Tight	N.A.	×	N.A.	N.A.	Fixed-point theorem; convex restriction
	[14]	✓	Loose	N.A.	×	N.A.	N.A.	Topological degree theorem
	[15] (LAIFT)	✓	Loose	N.A.	✓	Loose	N.A.	Mapping degree; implicit function theorem
	[16] (MDIMT)	✓	Loose	N.A.	✓	Loose	N.A.	Explicit inverse mapping theorem estimate
	This paper	×	**N.A.**	**N.A.**	✓	**Tight**	**Tight**	**Optimization (QCQP)**

*MDIMT denotes the explicit neighborhood-size estimate for the inverse mapping theorem in [16, Supplement 2.5A, Prop. 2.5.6], which is implemented as one of the comparison methods in Section VII.
*The inner bound on an HV solution neighborhood ensures that all PF solutions within it are unique, whereas the outer bound indicates a region where multiple mathematically valid PF solutions must exist for some inputs.

point for general networks. We make the following contributions.

▷ After presenting the modeling and settings in Section III, we exploit the quadratic structure of the PF equations in Cartesian coordinates in Section IV to show that finding the largest centered hyperrectangle with a prescribed aspect ratio is exactly equivalent to solving a collection of nonconvex quadratically constrained quadratic programs (QCQPs) whose number grows linearly with network size. To our knowledge, this provides the first exact characterization of largest unique-solution neighborhood of its kind.

▷ In Section V, we develop an inner approximation using semidefinite programming and quadratic-convex relaxations and an outer approximation using an interior-point method. We further develop a procedure for combining multiple certified HV neighborhoods into a larger, potentially nonconvex region while preserving injectivity of the PF mapping, in Section VI. The procedure certifies injectivity by verifying Jacobian non-singularity over the pairwise Minkowski averages of these neighborhoods.

▷ We conduct simulations on IEEE test systems to validate the proposed approach in Section VII. The results show that our approach identifies unique-solution neighborhoods up to two orders of magnitude larger than those obtained by state-of-the-art methods, and covers voltage ranges comparable to those encountered during normal operation.

We conclude the paper and discuss directions for future research in Section VIII.

II. RELATED WORK

There has been substantial work on the existence and uniqueness of PF solutions, with various approaches tailored to different network structures. This section provides a comprehensive review of existing studies, categorized based on network types as shown in Table I. We begin by noting conventional notations for bus types: the PV Bus (Generator Bus), characterized by known active power generation and voltage magnitude, the PQ Bus (Load Bus), defined by specified active and reactive power demand, and the Slack Bus, where the voltage magnitude and phase angle are predetermined. Since all power networks must have one slack bus, the categories are defined based on the remaining bus types as follows:

- **Distribution networks:** All PQ buses.
- **P-θ networks:** All PV buses.
- **General networks:** A mix of PQ and PV buses.

This categorization reflects the distinct characteristics and challenges of each network type, allowing for a structured analysis of the state-of-the-art in PF solution existence and uniqueness.

In the realm of distribution networks, several notable studies have employed fixed-point theorem approaches. The studies in [6]–[8] apply Banach's fixed-point theorem to derive explicit conditions for the existence and uniqueness of HV solutions. These methods formulate PF equations in a fixed-point form, exploring conditions under which the function is self-mapping and contractive. Recent work [9] employs tensor-based fixed-point formulations and shows that the unique fixed-point solution corresponds to the HV solution. While these approaches provide valuable insights, they often rely on specific network characteristics typical of distribution systems. Further advancing the analysis of distribution networks, the authors in [17] focus on radial networks, proving the existence and uniqueness of HV solutions under certain assumptions. Their work combines fixed-point methods, convex relaxation, and energy function approaches to demonstrate that all three methods identify the same HV solution. However, this study, while comprehensive, relies on strong assumptions of equal resistance-to-reactance ratios across all distribution lines, limiting its applicability to more general network configurations.

For P-θ networks, which are characterized by the presence of only PV nodes and bus phase angles being the only undetermined parameters, graph theory has been the primary tool for analysis. In [10], [11], uniqueness of PF solutions within a prescribed region is established by deriving graph-theoretic conditions under which the mapping from phase-angle differences to real power injections is (strictly) monotone over that region. The authors in [12] further exploit the cycle-space structure of meshed networks to derive a sufficient

condition for the existence and uniqueness of solutions to the lossless active PF equations. These methods offer scalability to large networks but are constrained by the specific structure of P-θ networks, which rarely occur in real-world power systems.

For general networks, the authors in [13] propose a monotone-operator approach for constructing convex domains in voltage space, each containing at most one PF solution. The topological degree theorem can also be used to study the existence of PF solutions within a given region [14]. The authors in [15] combine this result with the implicit function theorem to determine PF solution uniqueness regions. However, these methods rely on worst-case estimates and can therefore yield loose inner bounds, identifying regions less than 1% of the actual operating range, particularly as network size increases. More recently, [20] develops a holomorphic-based sufficient condition that guarantees the existence and uniqueness of an HV PF solution within a predefined voltage region. However, their formulation assumes fixed voltage phasors at generator buses rather than the conventional PV-bus model.

While previous studies provide useful insights for PF solution uniqueness, they often face limitations in practical applicability due to restrictive network assumptions and conservative estimates. These gaps motivate our proposed approach, which aims to leverage the fundamental results on quadratic functions and QCQPs to characterize maximum PF-solution uniqueness neighborhoods. By addressing the limitations of existing methods, our work seeks to advance the understanding of PF solution uniqueness in a manner that is both theoretically rigorous and practically relevant.

III. Modeling and Problem Statement

A. Power Network Model and Assumptions

We consider a balanced three-phase power network represented by its single-phase equivalent. The bus set is $\mathcal{N} := \{1, \dots, N\}$, with PV and PQ bus sets denoted by $\mathcal{G}$ and $\mathcal{D}$, respectively. The network branch set is $\mathcal{L} \subseteq \mathcal{N} \times \mathcal{N}$. We consider a single slack bus and, without loss of generality, buses $1, \dots, N-1$ are the non-slack buses and bus N is the slack bus, such that $\mathcal{N} = \mathcal{G} \cup \mathcal{D} \cup \{N\}$. The complex voltage at bus i is expressed in Cartesian voltage coordinates as $V_i = e_i + \mathrm{j} f_i$.

We assume that the slack, PV, and PQ bus types remain fixed throughout the PF calculation; in particular, bus-type switching due to reactive-power limits is not considered. The slack-bus complex voltage and PV-bus voltage magnitudes are specified. Without loss of generality, the slack-bus voltage is normalized as $e_N = 1$ and $f_N = 0$. The specified active-power injections at all non-slack buses and reactive-power injections at PQ buses are assumed to be independent of the bus voltages.

We also assume that the network topology and all transmission-line, transformer, and shunt parameters remain fixed during the PF calculation. In particular, transformer tap ratios and phase-shift angles are fixed rather than treated as PF variables. Treating them as variable control inputs would require extending the present PF model and is beyond the scope of this work. Fixed phase-shifting transformers are permitted, and hence the bus-admittance matrix $Y = G + \mathrm{j}B \in \mathbb{C}^{N \times N}$ need not be symmetric. Here, for branch $(i, j) \in \mathcal{L}$, G_{ij} and B_{ij} denote the conductance and susceptance components of Y_{ij}, respectively; $Y_{ij} = 0$ otherwise. The diagonal entries of Y include contributions from incident branches and bus shunts.

Remark 1 (Choice of voltage coordinates). The choice of Cartesian voltage coordinates is central to our analysis. In these coordinates, the PF mapping defined later is quadratic in the voltage variables, and its Jacobian is affine in them. This structure enables the exact QCQP characterization and tractable inner approximations developed later. In polar coordinates, by contrast, the PF mapping involves trigonometric nonlinearities, making analogous characterizations and approximations considerably more difficult to derive.

Remark 2 (Model generality). These assumptions define a standard class of AC PF models but are stronger than necessary for our analysis. We require only that the PF equations remain quadratic in Cartesian coordinates. Accordingly, our results extend to more general network and device models that preserve this quadratic structure.

B. Power Flow Problem, Power Flow Mapping, and Jacobian

The PF problem determines the bus voltages by solving a set of nonlinear PF equations, with the load demands at PQ buses and active power generation and voltage magnitudes at PV buses as inputs. Given a power network modeled above, the PF equations expressed in Cartesian coordinates are:

$$P_i = \sum_{k=1}^{N} \left[G_{ik}(e_i e_k + f_i f_k) + B_{ik}(f_i e_k - e_i f_k) \right], \; i \in \mathcal{D} \cup \mathcal{G}, \tag{1a}$$

$$Q_i = \sum_{k=1}^{N} \left[G_{ik}(f_i e_k - e_i f_k) - B_{ik}(e_i e_k + f_i f_k) \right], \; i \in \mathcal{D}, \tag{1b}$$

$$|V_i|^2 = e_i^2 + f_i^2, \; i \in \mathcal{G}. \tag{1c}$$

Equation (1a) represents the active power balance at PQ and PV buses, (1b) represents the reactive power balance at PQ buses, and (1c) describes the voltage magnitude relationship at PV buses. Given the known variables on the left-hand side (LHS) of (1), we can then calculate the unknown variables e_i and f_i for $i \in \mathcal{D} \cup \mathcal{G}$, which represent the non-slack-bus voltage profile over the power network, on the right-hand side (RHS) of (1). Note that the slack-bus voltage is fixed and does not appear as an unknown in (1). Once the PV- and PQ-bus voltages are obtained, the slack-bus injections and the remaining unknown $Q_i, i \in \mathcal{G}$ can also be determined by $e_i, f_i, i \in \mathcal{D} \cup \mathcal{G}$ through explicit calculations.

For ease of discussion later, we write the PF equations in (1) as a mapping from voltages to PF inputs as follows:

$$\mathbf{y} = g(\mathbf{v}), \tag{2}$$

where $\mathbf{y} \triangleq [P_i, Q_i, P_j, |V_j|^2, i \in \mathcal{D}, j \in \mathcal{G}]^\top \in \mathbb{R}^{2(N-1)}$ is the input vector, and $\mathbf{v} \triangleq [\tilde{\mathbf{e}}^\top, \tilde{\mathbf{f}}^\top]^\top \in \mathbb{R}^{2(N-1)}$ is the non-slack voltage vector with $\tilde{\mathbf{e}} = [e_i, i \in \mathcal{D} \cup \mathcal{G}]^\top$ and $\tilde{\mathbf{f}} = [f_i, i \in \mathcal{D} \cup \mathcal{G}]^\top$.

The mapping $g(\cdot)$ is quadratic (i.e., each entry of $\mathbf{y}$ is of degree at most 2 in the entries of $\mathbf{v}$) and the uniqueness of PF solutions corresponds to the *injectivity* of $g(\cdot)$, which means no two distinct voltage vectors $\mathbf{v}_1 \neq \mathbf{v}_2$ produce the same PF input $\mathbf{y}$. In the subsequent analysis, we primarily examine the properties of $g(\cdot)$ rather than the underlying equations. To facilitate this, we define the *Jacobian* of the PF mapping as a $2(N-1) \times 2(N-1)$ matrix below:

$$J_g(\mathbf{v}) = \frac{\partial g}{\partial \mathbf{v}}. \tag{3}$$

Since $g(\cdot)$ is quadratic, each entry of $J_g(\mathbf{v})$ is affine in $\mathbf{v}$. On an open convex region, a quadratic mapping is injective if and only if its Jacobian is nonsingular throughout the region, as we will discuss in detail in Section IV-A.

C. Problem Statement

In this paper, we seek the largest neighborhood around a reference HV operating point over which the PF mapping g is injective, thereby ensuring PF-solution uniqueness within the neighborhood. Let $\mathbf{v}_0 = [\mathbf{e}_0^\top, \mathbf{f}_0^\top]^\top$ denote a reference HV operating point, where $\mathbf{e}_0, \mathbf{f}_0 \in \mathbb{R}^{N-1}$ are the real and imaginary components of the non-slack bus voltages, respectively.[1] We assume that $J_g(\mathbf{v}_0)$ is nonsingular. In Cartesian coordinates, we restrict attention to open hyperrectangular *HV neighborhoods* centered at $\mathbf{v}_0$ with a prescribed aspect ratio $\kappa > 0$.[2] For $r > 0$, define

$$B(\mathbf{v}_0, \kappa, r) := \big\{\mathbf{v} = [\tilde{\mathbf{e}}^\top, \tilde{\mathbf{f}}^\top]^\top \in \mathbb{R}^{2(N-1)} \;\big|\; \|\tilde{\mathbf{e}} - \mathbf{e}_0\|_\infty < r, \quad \|\tilde{\mathbf{f}} - \mathbf{f}_0\|_\infty < \kappa r\big\}. \tag{4}$$

Figure 1 illustrates the neighborhood: $\mathbf{v}_0$ specifies its center, κ fixes its aspect ratio, and r controls its size. Specifically, r and κr are the half-widths along the real and imaginary voltage coordinates, respectively. For fixed $\mathbf{v}_0$ and κ, our objective is to determine the largest r for which g is injective on $B(\mathbf{v}_0, \kappa, r)$, which can be stated as the following problem.

$$r^*(\mathbf{v}_0, \kappa) \triangleq \max_{r>0} \; r \;\text{ s.t. }\; g \text{ is injective on } B(\mathbf{v}_0, \kappa, r). \tag{5}$$

We write $r^* = r^*(\mathbf{v}_0, \kappa)$ when the dependence on $\mathbf{v}_0$ and κ is clear. The following proposition establishes the existence of an optimal radius and characterizes its monotonicity properties. The corresponding set $B(\mathbf{v}_0, \kappa, r^*)$ is termed the *maximum unique-solution HV neighborhood*.

[1]Our focus on HV-solution uniqueness motivates choosing $\mathbf{v}_0$ within normal voltage operating ranges, e.g., $\sqrt{e_{0,i}^2 + f_{0,i}^2} \in [0.95, 1.05]$ p.u. for all non-slack buses. Nevertheless, our approach applies to any reference point $\mathbf{v}_0$ with nonsingular $J_g(\mathbf{v}_0)$.

[2]We adopt hyperrectangular HV neighborhoods rather than ℓ_2-norm balls because they yield componentwise linear constraints in Cartesian coordinates, thereby simplifying the resulting QCQP formulations developed in Section IV. Moreover, the Minkowski average of two hyperrectangles is itself a hyperrectangle, allowing the same neighborhood characterization to be used in the composition procedure developed in Section VI.

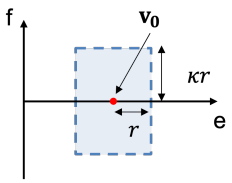


Fig. 1. Illustration of the open hyperrectangle HV neighborhood $B(\mathbf{v}_0, \kappa, r)$, centered at $\mathbf{v}_0$ with aspect ratio κ and size r; the boundary is excluded.

Proposition 1. *Recall that $J_g(\mathbf{v}_0)$ is nonsingular by setting. Suppose that $J_g(\mathbf{v})$ is singular for some $\mathbf{v} \in \mathbb{R}^{2(N-1)}$.*[3] *The following properties hold for $r^*(\mathbf{v}_0, \kappa)$:*

1) $0 < r^*(\mathbf{v}_0, \kappa) < \infty$, for any $\kappa > 0$.
2) $r^*(\mathbf{v}_0, \kappa)$ is non-increasing as κ increases.
3) $\kappa \cdot r^*(\mathbf{v}_0, \kappa)$ is non-decreasing as κ increases.

Proof. See Appendix A for a proof. □

Proposition 1 establishes that the maximum unique-solution HV neighborhood has a positive, finite radius for every prescribed aspect ratio $\kappa > 0$. It establishes the well-posedness of Problem (5), but does not directly provide a method for computing r^*. In Section IV, we exploit the quadratic structure of the PF mapping to derive an equivalent QCQP formulation.

Proposition 1 also states that the real-voltage half-width r^* is non-increasing, whereas the imaginary-voltage half-width κr^* is non-decreasing. The opposing trends in the two half-widths suggest that different choices of κ may yield nonnested neighborhoods, with no single aspect ratio necessarily producing a region that contains all others. This motivates combining certified HV neighborhoods with different aspect ratios and reference points to obtain larger, potentially nonconvex uniqueness regions, which we will discuss later in Section VI.

IV. Equivalent QCQP Formulations of the Maximum Unique-Solution HV Neighborhood

A. Jacobian Criterion for PF Mapping Injectivity

Solving Problem (5) requires determining whether the PF mapping is injective over a prescribed HV neighborhood, a condition that is difficult to verify directly.

The inverse function theorem [16] provides the familiar local result: for a continuously differentiable mapping, Jacobian nonsingularity at a point guarantees local invertibility, and hence local injectivity, near that point. For a general nonlinear mapping, however, it is known that Jacobian nonsingularity throughout an open convex set does not guarantee injectivity

[3]This assumption is mild. If the network contains a PV bus j, then $\partial|V_j|^2/\partial\mathbf{v} = \mathbf{0}^\top$ at $\mathbf{v} = \mathbf{0}$, making $J_g(\mathbf{0})$ singular. It also holds when a PF solution branch reaches a saddle-node loadability point [21]. The condition is therefore satisfied by a broad class of networks, including all test systems considered in this paper.

over the entire set.[4] Remarkably, for polynomial mappings of degree at most two, the local Jacobian criterion extends to any open convex set: the mapping is injective on the set if and only if its Jacobian is nonsingular throughout the set [24, Thm. 2.1].

We next specialize this result to the PF mapping g over the HV neighborhood $B(\mathbf{v}_0, \kappa, r)$, with a direct proof based on its quadratic structure for completeness.

Proposition 2. *For any $\kappa, r > 0$, the quadratic PF mapping $g : \mathbb{R}^{2(N-1)} \to \mathbb{R}^{2(N-1)}$ in Cartesian coordinates is injective on the open convex hyperrectangle $B(\mathbf{v}_0, \kappa, r)$ if and only if $J_g(\mathbf{v})$ is nonsingular for every $\mathbf{v} \in B(\mathbf{v}_0, \kappa, r)$.*

Proof. The results follow from [24, Thm. 2.1]; we give a simpler proof here for completeness. Since the PF mapping g is quadratic, J_g is affine. For any $\mathbf{v}_1, \mathbf{v}_2 \in B(\mathbf{v}_0, \kappa, r)$, it is straightforward to verify

$$g(\mathbf{v}_1) - g(\mathbf{v}_2) = J_g\left(\frac{\mathbf{v}_1 + \mathbf{v}_2}{2}\right)(\mathbf{v}_1 - \mathbf{v}_2).$$

If J_g is nonsingular throughout $B(\mathbf{v}_0, \kappa, r)$, convexity ensures that the midpoint lies in the neighborhood and thus its Jacobian is nonsingular; hence, $g(\mathbf{v}_1) = g(\mathbf{v}_2)$ implies $\mathbf{v}_1 = \mathbf{v}_2$.

Conversely, if $J_g(\mathbf{v}')$ is singular at some point in the neighborhood, choose $\mathbf{d} \neq \mathbf{0}$ such that $J_g(\mathbf{v}')\mathbf{d} = \mathbf{0}$. Openness ensures that $\mathbf{v}' \pm \epsilon\mathbf{d}$ remain in the neighborhood for sufficiently small $\epsilon > 0$. The identity above then gives $g(\mathbf{v}' + \epsilon\mathbf{d}) = g(\mathbf{v}' - \epsilon\mathbf{d})$, so g is not injective. □

Proposition 2 replaces the injectivity constraint in Problem (5) with the equivalent requirement of Jacobian nonsingularity throughout $B(\mathbf{v}_0, \kappa, r)$. Consequently, the maximum radius is determined by the first Jacobian singularity encountered as the hyperrectangle expands. We formalize this observation and derive equivalent formulations for computing $r^*(\mathbf{v}_0, \kappa)$.

Proposition 3. *Under the assumptions of Proposition 1, for any $\kappa > 0$, the following optimization problems attain the same optimal value $r^*(\mathbf{v}_0, \kappa) \in (0, \infty)$ as Problem* (5)*:*

$$\max_{r>0} \; r \text{ s.t. } J_g(\mathbf{v}) \text{ is nonsingular for all } \mathbf{v} \in B(\mathbf{v}_0, \kappa, r), \tag{6a}$$

$$\min_{r>0,\,\mathbf{v}} \; r \text{ s.t. } J_g(\mathbf{v}) \text{ is singular at some } \mathbf{v} \in \operatorname{cl} B(\mathbf{v}_0, \kappa, r), \tag{6b}$$

$$\min_{r>0,\,\mathbf{v},\,\mathbf{z}} \; r \;\text{ s.t. } J_g(\mathbf{v})\mathbf{z} = \mathbf{0}, \|\mathbf{z}\|_\infty = 1, \mathbf{v} \in \operatorname{cl} B(\mathbf{v}_0, \kappa, r). \tag{6c}$$

Here, $\mathbf{v}, \mathbf{z} \in \mathbb{R}^{2(N-1)}$, and $\operatorname{cl} B(\mathbf{v}_0, \kappa, r)$ denotes the closure of $B(\mathbf{v}_0, \kappa, r)$, obtained by replacing the strict inequalities in (4) *with non-strict inequalities.*

Proof. The equivalence between (5) and (6a) follows from Proposition 2. Moreover, r^* is the smallest radius for which $\operatorname{cl} B(\mathbf{v}_0, \kappa, r)$ contains a Jacobian singularity, establishing (6b). Finally, a matrix is singular if and only if it has a nonzero null vector, which can be normalized to satisfy $\|\mathbf{z}\|_\infty = 1$; hence, (6b) and (6c) are equivalent. □

We adopt Problem (6c) for the subsequent analysis. Since $J_g(\mathbf{v})$ is affine in $\mathbf{v}$, $J_g(\mathbf{v})\mathbf{z} = \mathbf{0}$ comprises nonconvex bilinear equality constraints, while $\mathbf{v} \in \operatorname{cl} B(\mathbf{v}_0, \kappa, r)$ is described by linear inequalities. The normalization $\|\mathbf{z}\|_\infty = 1$ can be decomposed into finitely many linearly described hypercube faces.[5] Together, these representations yield a number of nonconvex QCQPs that grows linearly with the network size.

B. Facetwise QCQP Reformulation

We first decompose the normalization constraint $\|\mathbf{z}\|_\infty = 1$. This constraint defines the boundary of the $2(N-1)$-dimensional unit hypercube, which comprises $4(N-1)$ facets. However, each pair of opposite facets yields the same optimal value: if $\mathbf{z}$ satisfies $J_g(\mathbf{v})\mathbf{z} = \mathbf{0}$, then so does $-\mathbf{z}$. It therefore suffices to consider the $2(N-1)$ facets

$$z_t = 1, \qquad -1 \le z_k \le 1, \quad k = 1, \dots, 2(N-1),$$

indexed by $t = 1, \dots, 2(N-1)$. Consequently, r^* is obtained by solving one nonconvex QCQP for each of the $2(N-1)$ facets and selecting the smallest optimal value:

$$r^* = \min_{t=1,\dots,2(N-1)} r_t^*, \tag{7}$$

where r_t^* is the positive square root of the optimum of the following QCQP problem:

$$\begin{aligned}
\min \quad & r_t^2 && \text{(8a)}\\
\text{s.t.} \quad & J_g(\mathbf{v})\mathbf{z} = \mathbf{0}, && \text{(8b)}\\
& |e_i - e_{0,i}| \le r_t, i = 1, \dots, N-1 && \text{(8c)}\\
& |f_i - f_{0,i}| \le \kappa \cdot r_t, i = 1, \dots, N-1 && \text{(8d)}\\
& -1 \le z_k \le 1,\ k = 1, \dots, 2(N-1) && \text{(8e)}\\
& z_t = 1, && \text{(8f)}\\
& e_N = 1,\ f_N = 0, && \text{(8g)}\\
\text{var.} \quad & \mathbf{e} = [e_i,\ i = 1, \dots, N]^\top \in \mathbb{R}^N, && \text{(8h)}\\
& \mathbf{f} = [f_i,\ i = 1, \dots, N]^\top \in \mathbb{R}^N, && \text{(8i)}\\
& \mathbf{z} = [z_i,\ i = 1, \dots, 2(N-1)]^\top \in \mathbb{R}^{2(N-1)}, && \text{(8j)}\\
& r_t \ge 0. && \text{(8k)}
\end{aligned}$$

In this QCQP formulation, κ and $\mathbf{v}_0$ are fixed parameters, while r_t is the radius of the HV neighborhood. Since $r_t \ge 0$, minimizing r_t^2 is equivalent to minimizing r_t and is convenient for the relaxations developed next. The equality constraint (8b) represents the singularity condition of the Jacobian matrix. Since each element of $J_g(\mathbf{v})$ is linear with respect to the decision variables $\mathbf{e}$ and $\mathbf{f}$, (8b) forms a set of nonconvex quadratic equality constraints. All remaining constraints are linear in the decision variables. Constraints (8c)–(8d) define

[4] For example, the exponential mapping $\Gamma(x, y) = (e^x \cos y, e^x \sin y)$ has an invertible Jacobian over the entire plane (an open convex set) since $\det J_\Gamma(x, y) = e^{2x} > 0$. Yet $\Gamma(x, y)$ is non-injective, as $\Gamma(x_0, y_0 + 2k\pi) = \Gamma(x_0, y_0)$ for every integer k. For polynomial mappings, a related and generally-incorrect Jacobian conjecture asks whether a nonzero constant Jacobian determinant guarantees global invertibility, and hence global injectivity [22]. While it does hold for quadratic and linear mappings [23], it does not apply to our PF setting as the corresponding Jacobian determinant is not constant.

[5] Because $J_g(\mathbf{v})\mathbf{z} = \mathbf{0}$ is homogeneous in $\mathbf{z}$, any nonzero null vector can be normalized. We choose the ℓ_∞-normalization on $\mathbf{z}$ because it yields linear facet constraints and explicit componentwise bounds on $\mathbf{z}$, which facilitate the construction of the McCormick envelopes in Section V-A. In contrast, the ℓ_2-normalization introduces the nonconvex equality $\mathbf{z}^\top\mathbf{z} = 1$.

$\mathrm{cl}\, B(\mathbf{v}_0, \kappa, r_t)$, (8e)–(8f) select a facet of $\|\mathbf{z}\|_\infty = 1$, and (8g) fixes the slack-bus voltage. Solving (8) for all $2(N-1)$ facets and taking the smallest optimum yields r^*.

The optimization problem (7) determines the minimum radius r^* among all subproblems indexed by t. Under the assumptions of Proposition 1, Proposition 3 establishes that this minimum exists and is finite, i.e., $r^* \in (0, \infty)$. While this guarantees the existence of a global solution, it does not imply feasibility of every subproblem (8). For any infeasible subproblem, we set $r_t^* = \infty$ by convention. However, the existence of finite r^* ensures that at least one subproblem (8) must be feasible, as r^* is the minimum of all r_t^*. We note that this approach can be adapted to characterize unique-solution regions for general quadratic mappings, broadening its potential applications.

We remark that the QCQP formulations in (8) provide an exact characterization of the maximum unique-solution HV neighborhood. To our knowledge, this is the first exact characterization of such a PF uniqueness neighborhood. Meanwhile, the difficulty of solving these nonconvex QCQPs globally motivates the inner and outer approximations developed next.

V. Inner and Outer Bounds on $B(\mathbf{v}_0, \kappa, r^*)$

In this section, we introduce a combination of semidefinite programming (SDP) and quadratic-convex (QC) relaxations to compute an inner bound of the maximum unique-solution HV neighborhood. An outer bound can be obtained by applying an interior-point method to obtain feasible points of the original QCQPs. The inner bound represents a certified voltage region over which the PF mapping is injective, thereby ensuring that each PF input has at most one solution within the region. Meanwhile, the outer bound indicates how large such a unique-solution neighborhood can be.

A. Computing an Inner Bound by SDP-QC Relaxation

Computing an inner bound on the maximum unique-solution HV neighborhood amounts to obtaining a lower bound on r^* in (7). Since $r^* = \min_{t=1,\dots,2(N-1)} r_t^*$, it suffices to obtain a lower bound on each subproblem optimal value in (8) and then take the minimum of these bounds. For each $t = 1, \dots, 2(N-1)$, we apply the SDP and QC relaxation techniques to the corresponding QCQP subproblem in (8) to obtain a lower bound on its optimal radius r_t^*. SDP relaxation is a powerful tool for obtaining lower bounds on the optimal values of QCQPs. However, due to the duality gap inherent in nonconvex problems, directly solving the SDP relaxation could result in overly conservative inner approximations. The QC relaxation involves substituting nonconvex sub-expressions with convex lower and upper bounds, known as convex envelopes. Specifically, we employ the *McCormick envelopes* for bilinear terms [25]. The combined SDP-QC relaxation generates a lower bound on the optimal value of the QCQP in (8) and is at least as tight as the bound obtained using the SDP relaxation alone [26].

Stack the decision variables of the QCQP problem in (8) into $\mathbf{x} = [\mathbf{e}^\top, \mathbf{f}^\top, \mathbf{z}^\top, r_t]^\top$, and denote the dimension of $\mathbf{x}$ by $N_x = 4N - 1$. The nonconvex constraints (8b) in (8) can be written as: for $k = 1, ..., 2(N-1)$,

$$\mathbf{x}^\top C^k \mathbf{x} + \mathbf{x}^\top D^k \mathbf{x} = \mathrm{Tr}(C^k \mathbf{x}\mathbf{x}^\top) + \mathrm{Tr}(D^k \mathbf{x}\mathbf{x}^\top) = 0,$$

where the constant matrices C^k and D^k for $k = 1, ..., 2(N-1)$ are well defined and can be calculated following a standard procedure according to the admittance matrix [27]. By substituting $\mathbf{x}\mathbf{x}^\top$ with a symmetric positive semidefinite matrix W, the above nonconvex constraints can be written as linear constraints with respect to W:

$$\mathrm{Tr}(C^k W) + \mathrm{Tr}(D^k W) = 0, k = 1, ..., 2(N-1).$$

Furthermore, to tighten the relaxation results, we bound the bilinear terms $e_i z_j$ and $f_i z_j$ ($i = 1, ..., N-1$ and $j = 1, ..., 2(N-1)$) that appear in the nonconvex constraint (8b) by using McCormick envelopes. For the reference point $\mathbf{v}_0 = [\mathbf{e}_0^\top, \mathbf{f}_0^\top]^\top$, the componentwise bounds are $e_i \in [e_{0,i} - r_t, e_{0,i} + r_t]$ and $f_i \in [f_{0,i} - \kappa r_t, f_{0,i} + \kappa r_t]$. Accordingly, the McCormick-envelope formulation is given by (10), with a detailed derivation specified in Appendix C. Denote the standard basis vectors in $\mathbb{R}^{N_x}$ by $\mathbf{i}_1, \mathbf{i}_2, \dots, \mathbf{i}_{N_x}$, where $N_x = 4N - 1$ is the dimension of the stacked variable $\mathbf{x}$. The remaining linear equality and inequality constraints in (8) can be written as linear functions of $\mathbf{x}$. Using the fact that $\mathbf{x} = W\mathbf{i}_N$,[6] and relaxing the constraint $\mathrm{rank}(W) = 1$, we obtain an SDP-QC relaxation for every QCQP in (8):

$$\min\ \mathrm{Tr}\left(\mathbf{i}_{N_x}\mathbf{i}_{N_x}^\top W\right) \tag{9a}$$
$$\text{s.t. } \mathrm{Tr}\left(C^k W\right) + \mathrm{Tr}\left(D^k W\right) = 0,\ k = 1, ..., 2(N-1) \tag{9b}$$
$$-\mathbf{i}_{N_x}^\top \mathbf{x} \le \mathbf{i}_i^\top \mathbf{x} - e_{0,i} \le \mathbf{i}_{N_x}^\top \mathbf{x}, i = 1, ..., N-1 \tag{9c}$$
$$-\kappa \cdot \mathbf{i}_{N_x}^\top \mathbf{x} \le \mathbf{i}_{i+N}^\top \mathbf{x} - f_{0,i} \le \kappa \cdot \mathbf{i}_{N_x}^\top \mathbf{x}, i = 1, ..., N-1 \tag{9d}$$
$$-1 \le \mathbf{i}_{i+2N}^\top \mathbf{x} \le 1,\ i = 1, ..., 2(N-1) \tag{9e}$$
$$\mathbf{i}_{(t+2N)}^\top \mathbf{x} = 1, \tag{9f}$$
$$\mathbf{i}_N^\top \mathbf{x} = 1,\ \mathbf{i}_{2N}^\top \mathbf{x} = 0, \tag{9g}$$
$$\mathbf{i}_{N_x}^\top \mathbf{x} \ge 0, \tag{9h}$$
$$\mathbf{x} = W\mathbf{i}_N, \tag{9i}$$
$$W \succeq 0, \tag{9j}$$
$$\text{constraints in (10)}, i = 1, ..., N-1, j = 1, ..., 2(N-1), \tag{9k}$$
$$\text{var. } \mathbf{x} \in \mathbb{R}^{N_x},\ W \in \mathbb{S}^{N_x}. \tag{9l}$$

In the above problem, W, C^k, and D^k are $N_x \times N_x$ matrices. The objective (9a) is an equivalent formulation of (8a) and is linear in the decision variable W. The optimal objective value provides a lower bound on $(r_t^*)^2$. Constraints (9b)–(9j) constitute the standard SDP relaxation. By substituting the decision variables, constraints (9b) are equivalent to (8b), and also are linear with respect to W. Constraints (9c)–(9h) are exact formulations of the remaining linear constraints in (8). Constraint (9i) describes the relationship between $\mathbf{x}$ and W.

[6] Bus N is the slack bus, so the N-th component of $\mathbf{x}$ is $x_N = e_N = 1$. Since $W = \mathbf{x}\mathbf{x}^\top$ and $\mathbf{i}_N$ is the N-th standard basis vector, $W\mathbf{i}_N = \mathbf{x}\mathbf{x}^\top \mathbf{i}_N = \mathbf{x} x_N = \mathbf{x}$.

$$
\begin{cases}
W_{(i)(j+2N)} \geq -W_{(N_x)(j+2N)} + e_{0,i}W_{(N)(j+2N)} - W_{(N)(i)} - W_{(N)(N_x)} + e_{0,i}, \\
W_{(i)(j+2N)} \geq W_{(N_x)(j+2N)} + e_{0,i}W_{(N)(j+2N)} + W_{(N)(i)} - W_{(N)(N_x)} - e_{0,i}, \\
W_{(i)(j+2N)} \leq W_{(N_x)(j+2N)} + e_{0,i}W_{(N)(j+2N)} - W_{(N)(i)} + W_{(N)(N_x)} + e_{0,i}, \\
W_{(i)(j+2N)} \leq -W_{(N_x)(j+2N)} + e_{0,i}W_{(N)(j+2N)} + W_{(N)(i)} + W_{(N)(N_x)} - e_{0,i},
\end{cases}
$$

$$
\begin{cases}
W_{(i+N)(j+2N)} \geq -\kappa W_{(N_x)(j+2N)} + f_{0,i}W_{(N)(j+2N)} - W_{(N)(i+N)} - \kappa W_{(N)(N_x)} + f_{0,i}, \\
W_{(i+N)(j+2N)} \geq \kappa W_{(N_x)(j+2N)} + f_{0,i}W_{(N)(j+2N)} + W_{(N)(i+N)} - \kappa W_{(N)(N_x)} - f_{0,i}, \\
W_{(i+N)(j+2N)} \leq \kappa W_{(N_x)(j+2N)} + f_{0,i}W_{(N)(j+2N)} - W_{(N)(i+N)} + \kappa W_{(N)(N_x)} + f_{0,i}, \\
W_{(i+N)(j+2N)} \leq -\kappa W_{(N_x)(j+2N)} + f_{0,i}W_{(N)(j+2N)} + W_{(N)(i+N)} + \kappa W_{(N)(N_x)} - f_{0,i}.
\end{cases}
\tag{10}
$$

Constraints (9k) are the convex envelopes for the bilinear terms $e_i z_j$ and $f_i z_j$, which are a sequence of inequality constraints linear in W. The inclusion of constraints (9k) is crucial for tightening the bounds beyond what the SDP relaxation alone can achieve. The relaxed problem in (9) is convex and its optimal objective value provides a lower bound on that of the QCQP problem in (8). After solving the relaxed problem in (9), if the rank of the matrix W is equal to 1, then the solution is the global optimum of the original QCQP problem in (8) [28]. By solving (9) for each $t = 1, \ldots, 2(N-1)$ and taking the minimum of the square roots of the resulting optimal values, we obtain an inner bound $r_{\text{in}} \leq r^*$ on the optimal radius r^* in (7).[7] If at least one SDP-QC subproblem attaining the minimum that defines r_{in} has a rank-one optimal matrix W^*, then $r_{\text{in}} = r^*$. Otherwise, exactness is not certified, and r_{in} may be conservative.

Computational complexity: Recall that N is the number of buses. The dimension of the positive semidefinite matrix in the SDP formulation above is $\mathcal{O}(N)$, and the number of constraints is $\mathcal{O}(N^2)$. The computational complexity of solving this SDP problem by interior-point methods is then $\mathcal{O}(N^{5.246})$ [29]. We need to solve the SDP problem (9) $\mathcal{O}(N)$ times and select the minimal r_t to find the inner bound of the maximum unique-solution HV neighborhood. Thus the overall complexity of finding an inner bound is $\mathcal{O}(N^{6.246})$[8].

B. Computing an Outer Bound by Interior-Point Method

The overall problem (7) is designed to identify the smallest HV-neighborhood radius at which a Jacobian singularity is encountered. Consequently, any feasible solution of the t-th subproblem (8) provides an upper bound on its optimal value r_t^*. Since $r^* = \min_{t=1,\ldots,2(N-1)} r_t^*$, replacing each r_t^* with such an upper bound yields an upper bound r_{out} on r^*, and hence an outer bound on $B(\mathbf{v}_0, \kappa, r^*)$. To find an outer bound that is as tight as possible, we employ the interior-point method to solve every subproblem (8) and take the minimum of the resulting feasible objective values over $t = 1, \ldots, 2(N-1)$. Even with locally optimal solutions, this approach serves to provide a valid outer bound for the maximum unique-solution HV neighborhood. To tighten the bound, we utilize different initial points to warm-start the interior-point solver, which increases the likelihood of finding a tight bound by exploring various regions of the solution space.

Computational complexity: For each subproblem (8), suppose we employ L different initial points to warm start the solver. Assuming these warm-start points lead to local optima, and denoting the number of iterations as M, each iteration has computational complexity $\mathcal{O}(N^3)$ [30]. Consequently, the overall computational complexity for master problem (7) is $\mathcal{O}(LMN^4)$.

This outer bound procedure, combined with the inner bound approximation described earlier, provides a comprehensive characterization of the maximum unique-solution HV neighborhood $B(\mathbf{v}_0, \kappa, r^*)$. The inner bound offers a guaranteed region of uniqueness, while the outer bound delimits the potential extent of this region. Together, they enhance our understanding of the behavior of PF solutions in the vicinity of the operating point, and are useful for analyzing system stability and operational limits.

Next, we develop a procedure for combining multiple open, convex, and certified HV neighborhoods into a larger region while preserving injectivity of the PF mapping.

VI. Combining Multiple Certified HV Neighborhoods while Preserving Injectivity

The preceding sections developed nonconvex QCQP formulations that exactly characterize the largest centered HV uniqueness hyperrectangle with a prescribed aspect ratio in Cartesian voltage coordinates, together with methods for computing inner and outer bounds on its size. A natural next question is whether certified hyperrectangles with different centers and/or aspect ratios can be combined into a larger, potentially nonconvex region. Because injectivity on each hyperrectangle does not guarantee injectivity on their union [9], this section develops a composition procedure that preserves PF-mapping injectivity. We also provide an outer approximation that bounds the possible extent of the composite region.

The following results present a *sufficient* condition for certifying injectivity of g over unions of solution-uniqueness neighborhoods, as long as each of them is open and convex, based on pairwise Minkowski averages [31].

[7] To obtain the lower bound on r^* in (7), it is sufficient to solve $2(N-1)$ instances of subproblem (9). To tighten the inner bound, we exploit the sign symmetry of Problem (8): fixing $z_t = 1$ or $z_t = -1$ yields the same optimal value. Thus, for each $t = 1, \ldots, 2(N-1)$, we solve Problem (9) for both $\mathbf{i}_{(t+2N)}^\top \mathbf{x} = 1$ and $\mathbf{i}_{(t+2N)}^\top \mathbf{x} = -1$ in constraint (9f), and retain the larger of the two as a valid lower bound on r_t^*.

[8] All computational complexity expressions discussed in this work omit the term $\log(1/\epsilon)$, where $\epsilon > 0$ is the accuracy parameter.

[9] For example, for two unique-solution HV neighborhoods B_i and B_j, there may exist $\mathbf{v}_1 \in B_i$ and $\mathbf{v}_2 \in B_j$, with $i \neq j$, such that $g(\mathbf{v}_1) = g(\mathbf{v}_2)$.

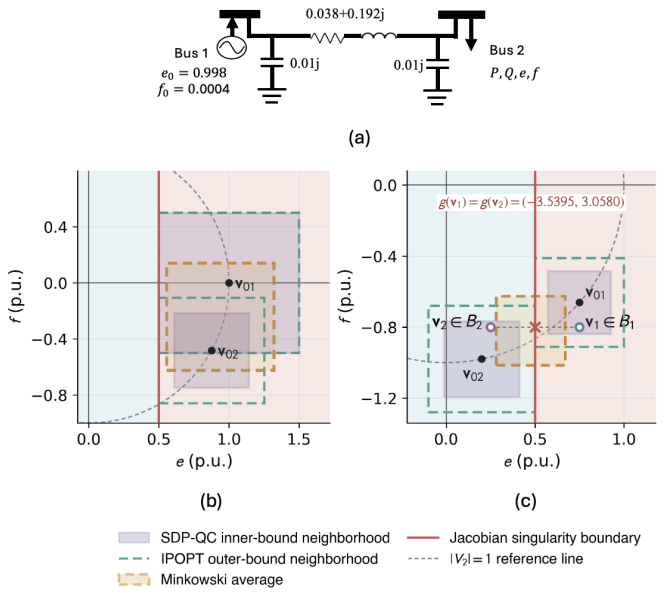


Fig. 2. Composition of HV neighborhoods in a two-bus example. (a) Network model. In (b) and (c), the blue and red regions denote low- and high-voltage solutions, respectively, separated by the Jacobian singularity boundary. (b) A composable pair whose Minkowski average avoids the boundary. (c) A noncomposable pair whose average intersects the boundary and whose union is noninjective.

Theorem 1 (Injectivity of Unions)**.** *Let $\{B_i\}_{i=1}^m (m \geq 2)$ be a finite collection of open and convex HV neighborhoods, such that the PF mapping g is injective on each B_i. If $J_g(\mathbf{v})$ is nonsingular for each $\mathbf{v}$ in the Minkowski average set*

$$\frac{1}{2}(B_i + B_j) := \left\{ \frac{1}{2}(\mathbf{v}_i + \mathbf{v}_j) \mid \mathbf{v}_i \in B_i,\ \mathbf{v}_j \in B_j \right\} \quad (11)$$

for every pair $i \neq j$, then g is injective on $\bigcup_{i=1}^m B_i$.

Proof. See Appendix B for the complete proof. Here we provide a proof sketch. The theorem follows intuitively from the midpoint identity for quadratic mappings:

$$g(\mathbf{v}_i) - g(\mathbf{v}_j) = J_g\left(\frac{\mathbf{v}_i + \mathbf{v}_j}{2}\right)(\mathbf{v}_i - \mathbf{v}_j).$$

Injectivity within each B_i holds by assumption. For points in different B_i and B_j, their midpoint lies in $\frac{1}{2}(B_i + B_j)$. Jacobian nonsingularity on this set therefore prevents distinct points from having the same image under g. □

The theorem provides a pairwise certificate for combining neighborhoods with different centers and aspect ratios into a larger, potentially nonconvex uniqueness region. Although the condition is not necessary for every particular union, it is essential in a worst-case sense: when it fails, injectivity of the union is no longer guaranteed. Figure 2(c) illustrates two individually injective hyperrectangles for which the condition fails and the PF mapping is not injective on their union.

Combining multiple certified hyperrectangles: The Minkowski average of two hyperrectangles is itself a hyperrectangle and can therefore be analyzed using Sections IV and V. For $B_i := B(\mathbf{v}_{0i}, \kappa_i, r_i)$ and $B_j := B(\mathbf{v}_{0j}, \kappa_j, r_j)$,

$$(B_i + B_j)/2 = B(\bar{\mathbf{v}}_{0ij}, \bar{\kappa}_{ij}, \bar{r}_{ij}),$$

Algorithm 1: Constructing a Certified Composite HV Region

Require: Parameter pairs $\{(\mathbf{v}_{0i}, \kappa_i)\}_{i=1}^m$.
Ensure: Radii $\{r_i\}_{i=1}^m$ such that g is injective on $\mathcal{B} = \bigcup_{i=1}^m B(\mathbf{v}_{0i}, \kappa_i, r_i)$.

for $i = 1, \ldots, m$ **do**
  $r_i \leftarrow r^*(\mathbf{v}_{0i}, \kappa_i)$.
end for
for each pair $i < j$ **do**
  Using the current r_i and r_j, compute $\bar{\mathbf{v}}_{0ij}$, $\bar{\kappa}_{ij}$, and $\bar{r}_{ij}$ via (12).
  $r_{ij}^* \leftarrow r^*(\bar{\mathbf{v}}_{0ij}, \bar{\kappa}_{ij})$.
  if $r_{ij}^* < \bar{r}_{ij}$ **then**
    $\tau \leftarrow r_{ij}^*/\bar{r}_{ij}$.
    $r_i \leftarrow \tau r_i, \quad r_j \leftarrow \tau r_j$.
  end if
end for
$\widehat{B}_i \leftarrow B(\mathbf{v}_{0i}, \kappa_i, r_i)$, for all $i = 1, \ldots, m$.
return $\mathcal{B} \leftarrow \bigcup_{i=1}^m \widehat{B}_i$.

Note: In implementation, each evaluation of r^* is replaced by its SDP-QC lower bound r_{in} from Section V-A.

where

$$\bar{\mathbf{v}}_{0ij} = \frac{\mathbf{v}_{0i} + \mathbf{v}_{0j}}{2},\ \bar{r}_{ij} = \frac{r_i + r_j}{2},\ \bar{\kappa}_{ij} = \frac{\kappa_i r_i + \kappa_j r_j}{r_i + r_j}. \quad (12)$$

Thus, the pair satisfies the condition of Theorem 1 if $r^*(\bar{\mathbf{v}}_{0ij}, \bar{\kappa}_{ij}) \geq \bar{r}_{ij}$.

Algorithm 1 checks all $\mathcal{O}(m^2)$ pairs using the SDP-QC lower bounds on the corresponding maximum radii from Section V-A. If a pair fails the test, its radii are reduced by a common factor until the sufficient condition holds; Appendix D determines the largest admissible factor. Because each reduction replaces a neighborhood by a subset, it preserves individual injectivity and all previously verified pairwise conditions. Consequently, after all pairwise checks, every pair of the remaining neighborhoods $\{\widehat{B}_i\}_{i=1}^m$ satisfies Theorem 1, and the PF mapping is injective on $\mathcal{B} := \bigcup_{i=1}^m \widehat{B}_i$.

Computational complexity: For m candidate neighborhoods, the certified construction requires m individual and $\binom{m}{2}$ pairwise SDP-QC computations, for a total of $\mathcal{O}(m^2)$ computations. Using the $\mathcal{O}(N^{6.246})$ complexity derived in Section V-A, the overall complexity is $\mathcal{O}(m^2 N^{6.246})$. These offline computations are partially parallelizable: all individual computations are independent, and pairwise tests with disjoint index pairs can be performed concurrently.

Outer approximation: For the same parameter pairs $\{(\mathbf{v}_{0i}, \kappa_i)\}_{i=1}^m$, define

$$\mathcal{B}^{\text{out}} := \bigcup_{i=1}^m B(\mathbf{v}_{0i}, \kappa_i, r_{i,\text{out}}),$$

where $r_{i,\text{out}}$ is an upper bound on $r^*(\mathbf{v}_{0i}, \kappa_i)$ obtained using the interior-point method in Section V-B. This union bounds the possible extent of the composite region but is not itself certified to be injective. Because no pairwise verification is required, its construction involves m independent computations, each of which incurs a complexity of $\mathcal{O}(LMN^4)$, as established in Section V-B. The total complexity is thus $\mathcal{O}(mLMN^4)$.

Figure 2 illustrates the composition procedure using the two-bus system in panel (a). In Figure 2(b) and Figure 2(c), B_i, $i \in \{1, 2\}$, denotes the SDP-QC inner-bound neighborhood centered at $\mathbf{v}_{0i}$ with $\kappa = 1$, shown as a purple square.

In Figure 2(b), both bounds recover the exact radius at $\mathbf{v}_{01}$, whereas only the interior-point outer bound is exact at $\mathbf{v}_{02}$. Nevertheless, the Minkowski average $\frac{1}{2}(B_1 + B_2)$ contains no Jacobian singularity; hence, Theorem 1 certifies injectivity of g on $B_1 \cup B_2$. In Figure 2(c), the Minkowski average intersects the singularity boundary, so the composition condition fails. Indeed, distinct points $\mathbf{v}_1 \in B_1$ and $\mathbf{v}_2 \in B_2$ satisfy $g(\mathbf{v}_1) = g(\mathbf{v}_2)$, with their midpoint on the singularity boundary, proving that g is not injective on $B_1 \cup B_2$.

VII. Numerical Experiments

This section evaluates the proposed inner- and outer-bound methods on IEEE test systems through three sets of experiments. We first describe the experiment setup in the first subsection. The second subsection compares the certified neighborhoods centered at the flat-start point with existing methods and assesses computational performance. For a fixed reference point $\mathbf{v}_0$, the third subsection examines how the aspect ratio κ affects the neighborhoods and quantifies the enlargement achieved by composing neighborhoods with different aspect ratios. The last subsection considers different reference points and demonstrates how their composition expands the certified region to cover a broader range of operating conditions.

A. Experiment Setup

We consider multiple IEEE test cases available in MATPOWER [32]. To reduce computational complexity without losing characterization accuracy, we apply Kron reduction [33] to obtain a reduced admittance matrix, which is then used to formulate both inner and outer approximation problems.

The optimization problem is solved by using YALMIP [34], a high-level MATLAB toolbox for modeling and solving optimization problems. We utilize Mosek [35] as the SDP solver for the SDP-QC inner-bound problem in (9), and IPOPT [36] as the interior-point solver for obtaining an outer bound for the nonconvex QCQP problem in (8). To tighten the SDP-QC inner bound, we solve (9) twice for each t, imposing $\mathbf{i}_{t+2N}^\top \mathbf{x} = 1$ and $\mathbf{i}_{t+2N}^\top \mathbf{x} = -1$ in constraint (9f), respectively, and retain the larger of the two lower bounds on r_t^* (see discussion in Footnote 7). To obtain tight outer bounds, we employ multiple warm-start conditions and choose the tightest outer bound observed. These initial points include the SDP-QC inner-bound results, flat-start point, and 50 random states.[10] All experiments were run on a server with two AMD EPYC 9754 CPUs (512 logical cores, 1.5 TiB RAM in total).

For comparative analysis, we benchmark our methods against two established schemes for certifying local uniqueness regions:

- **MDIMT**: The explicit estimate for the size of the neighborhoods in the inverse mapping theorem given in [16, Supplement 2.5A, Prop. 2.5.6]. It uses $L = \|Dg(\mathbf{v}_0)\|$, $M = \|Dg(\mathbf{v}_0)^{-1}\|$, and an upper bound K on $\|D^2 g(\mathbf{v})\|$ over a prescribed neighborhood to construct a guaranteed local injectivity region. We implement this textbook estimate as the MDIMT comparison method.
- **LAIFT**: The mapping-degree-based local estimate in [15] for the domains of validity of the inverse and implicit function theorems. It also uses first- and second-order derivative information to obtain an inner bound around a nonsingular operating point.

Both methods provide inner bounds on a local uniqueness region around a point of interest and are applicable to the PF mapping because $g(\mathbf{v})$ is a $\mathcal{C}^2$ quadratic mapping[11]. Unlike the proposed method, neither benchmark directly searches for the closest singularity of the PF Jacobian or characterizes the maximum unique-solution HV neighborhood.

B. Benchmark Comparison and Computational Performance

In this experiment, we compare the proposed method with the MDIMT and LAIFT baseline methods described in Section VII-A. The comparison is conducted on seven IEEE test systems, with the number of buses ranging from 5 to 141 and covering both transmission and distribution networks. For each test case, we fix the reference point $\mathbf{v}_0 = [\mathbf{1}^\top, \mathbf{0}^\top]^\top$, and set $\kappa = 1$. The size of each neighborhood is therefore characterized by its radius r. The proposed method computes inner bounds using SDP-QC relaxation in Section V-A and outer bounds using the interior-point method in Section V-B. The MDIMT and LAIFT methods provide only inner bounds.

Table II shows that the proposed inner bound exceeds the larger baseline bound in every case, by factors ranging from approximately 1.7 to 535 and beyond. The gain exceeds two orders of magnitude for the 30-/85-/141- bus systems. The smaller MDIMT and LAIFT bounds reflect the conservatism of uniform derivative estimates over prescribed domains. The proposed bounds satisfy $r_{\text{in}} \leq r^* \leq r_{\text{out}}$. The inner–outer bound gaps may arise from both sides. For the inner bounds, the lifted optimal matrices of the SDP-QC subproblems attaining the minimum are not rank one; therefore, exactness of the reported inner bounds cannot be certified. For the outer bounds, IPOPT may return feasible points whose objective values exceed the global minimum. Because (7)–(8) exactly characterize r^*, stronger relaxation hierarchies may further narrow these gaps [37].

Figure 3 reports solver times accumulated over all subproblems, while Table III reports the corresponding per-subproblem means and standard deviations. Each outer-bound subproblem aggregates 52 IPOPT runs with different initializations. MDIMT and LAIFT are omitted because their analytical evaluations have negligible cost.[12]

[10] The flat-start point is defined as $\mathbf{v}_0 = [\mathbf{1}^\top, \mathbf{0}^\top]^\top$. The voltage components $\mathbf{e}$ and $\mathbf{f}$ are uniformly sampled within ± 0.3 p.u. of flat-start point, auxiliary variables $\mathbf{z}$ are uniformly sampled between -1 and 1, while keeping the variable r_t initialized at 0.

[11] A function h is $\mathcal{C}^2$ if both h and its first derivative h' are continuously differentiable.

[12] Three independent repetitions with different random seeds produced negligible variation relative to the reported runtimes.

TABLE II
COMPARISON OF THE SIZE OF THE UNIQUE-SOLUTION HV NEIGHBORHOOD COMPUTED BY DIFFERENT SCHEMES ($\kappa = 1, \mathbf{v}_0 = [\mathbf{1}^\top, \mathbf{0}^\top]^\top$).

Network Type	**# Buses**	**Radius r (p.u.)**			
		Proposed Method		**Existing Methods (Inner Bounds)**	
		Inner Bound	**Outer Bound**	**MDIMT**	**LAIFT**
Transmission	5	0.132	0.274	0.077	2.20×10^{-3}
	9	0.118	0.255	0.025	4.72×10^{-3}
	14	0.051	0.143	0.011	2.61×10^{-3}
	30	0.054	0.111	3.30×10^{-3}	0.477×10^{-3}
	57	0.016	0.056	0.969×10^{-3}	0.345×10^{-3}
Distribution	85	0.015	0.0176	0.074×10^{-3}	0.028×10^{-3}
	141	0.020	0.0218	0.512×10^{-3}	$< 10^{-6}$

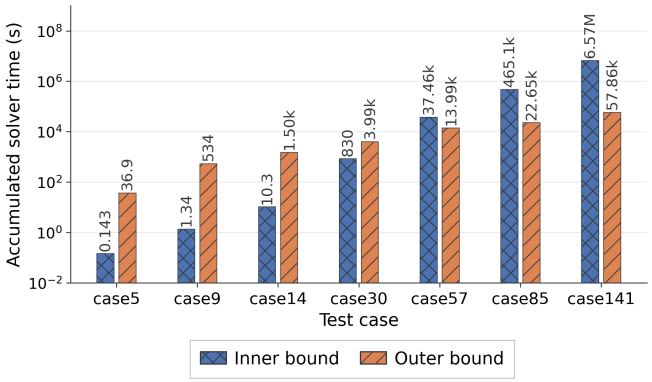


Fig. 3. Runtime comparison of the inner- and outer-bound computations for the proposed method.

TABLE III
PER-SUBPROBLEM SOLVING TIME FOR THE INNER- AND OUTER-BOUND COMPUTATIONS, ON AN AMD EPYC 9754 CPU.

# Buses	**Inner-bound time (s)**	**Outer-bound time (s)**
5	0.0179 ± 0.0016	4.61 ± 1.14
9	0.0841 ± 0.0107	33.37 ± 22.20
14	0.431 ± 0.075	62.48 ± 40.51
30	18.05 ± 2.38	86.73 ± 56.26
57	456.77 ± 78.72	170.66 ± 82.69
85	$4,009.83 \pm 397.24$	195.25 ± 57.27
141	$39,089.20 \pm 5,644.14$	344.42 ± 66.87

For systems with up to 30 buses, the multistart outer-bound computation is slower; from 57 buses onward, the SDP-QC inner-bound computation dominates. At 141 buses, their accumulated solving times on a single AMD EPYC 9754 CPU are $1,825$ and 16 hours, respectively, identifying the SDP relaxation as the main scalability bottleneck worthy for future investigations. On the practical side, while computing the inner bounds can be time consuming for large-scale power networks, these bounds are computed offline once per network and parameter pair $(\mathbf{v}_0, \kappa)$, and the independent subproblems can be solved in parallel, which can drastically reduce the time needed. Furthermore, GPU-accelerated SDP solvers [38] and chordal decomposition [39] may further improve scalability.

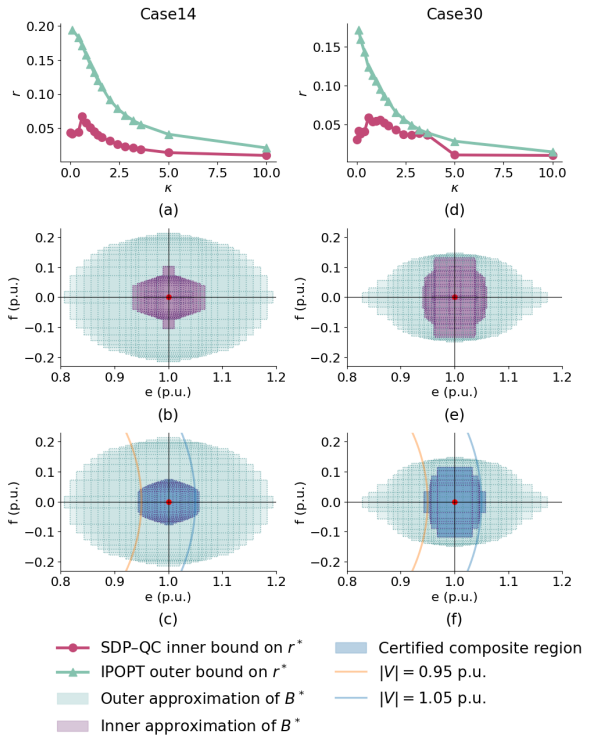


Fig. 4. The inner and outer approximations concerning different values of κ. Figures (a) and (d) show how inner and outer bounds on r change as κ increases. Figures (b) and (e) show different HV neighborhoods corresponding to different values of κ. The light blue regions represent the outer approximations, and the purple regions represent the inner approximations. Figures (c) and (f) show the certified composite regions obtained from the inner-bound neighborhoods (dark blue) and the outer-bound unions (light blue). The solid orange and blue lines represent the lower and upper voltage magnitude limits, respectively.

C. Aspect-Ratio Effects and Combination of Neighborhoods

We examine how the aspect ratio κ affects the maximum HV uniqueness neighborhood for the IEEE 14- and 30-bus systems. At the flat-start point $\mathbf{v}_0 = [\mathbf{1}^\top, \mathbf{0}^\top]^\top$, we compute inner and outer bounds on $r^*(\mathbf{v}_0, \kappa)$ over a discrete set of values satisfying $0 < \kappa \leq 10$.[13] Figure 4(a) and (d) report these bounds. The remaining panels project each high-

[13]Larger values produce increasingly narrow real-voltage ranges and highly elongated neighborhoods; the selected range captures the practically relevant tradeoff.

dimensional neighborhood onto a single-bus e–f plane. Each projected rectangle has horizontal and vertical half-widths r and κr, respectively. As these bounds are uniform across non-slack buses, the full neighborhood is the Cartesian product of identical rectangles.

The IPOPT outer bounds exhibit the tradeoff established in Proposition 1: r decreases while κr increases with κ. The SDP-QC inner bounds do not always preserve these monotonicity properties, reflecting relaxation gaps at some values of κ. Figure 4(b) and (e) show the projected inner neighborhoods in purple and outer neighborhoods in light blue. Their direct unions illustrate the geometric effects of varying κ but are not certified to be injective.

Figure 4(c) and (f) show the results of Algorithm 1. After pairwise Minkowski-average verification and any required shrinking, the dark-blue union is certified to preserve PF-mapping injectivity; the light-blue outer union bounds its possible extent but has no injectivity guarantee. We next quantify the change in area introduced by the composition procedure by computing the area of each projected union while counting overlapping portions only once. Relative to the largest single certified neighborhood, composition increases the projected area by 24.2% for the 14-bus system and 8.1% for the 30-bus system. Pairwise certification reduces the corresponding unverified inner-bound unions by only 20.8% and 19.3%, respectively. The solid curves indicate the normal voltage-magnitude limits $|V| = 0.95$ and 1.05 p.u.

As seen, the certified composite inner-bound regions are comparable in extent to the normal voltage operating range. Operationally, this could be encouraging: when a computed solution lies within such a region, operators can rule out competing HV solutions within the region for the same PF inputs, increasing confidence in PF-based security assessments and operational decisions.

D. Combination of Neighborhoods Across Different $\mathbf{v}_0$

We evaluate neighborhood composition across multiple reference points using the IEEE 30-bus system with $\kappa = 1$. We select a sequence of reference voltage profiles whose magnitudes remain at 1 p.u. while their phase angles vary. For each reference point, the SDP-QC relaxation provides a certified inner-bound radius, and the interior-point method provides an outer-bound radius. Algorithm 1 then verifies the pairwise Minkowski-average conditions and shrinks the inner neighborhoods when necessary.

Figure 5 displays the results on a representative single-bus e–f plane. Because $\kappa = 1$, each projected neighborhood is a square, and the varying phase angles place their centers along the unit-magnitude curve. The full neighborhoods are Cartesian products of these single-bus projections. In Figure 5(a), the purple and light-blue squares represent the individual inner- and outer-bound neighborhoods, respectively; the red marker denotes the flat-start voltage $(1, 0)$. Although each purple square is individually certified, their direct union is not necessarily injective. Figure 5(b) shows the neighborhoods remaining after pairwise verification and shrinking. Their dark-blue union is certified to preserve PF-mapping injectivity,

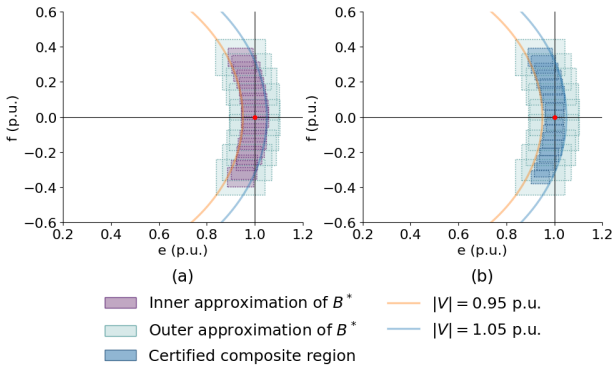


Fig. 5. (a) Inner and outer bounds of the maximum unique-solution HV neighborhoods for different $\mathbf{v}_0$ in the IEEE 30-bus system. (b) Certified composite region with a unique-solution guarantee and its outer approximation.

whereas the light-blue union only bounds its possible extent. Again, the solid curves indicate the normal voltage-magnitude limits $|V| = 0.95$ and 1.05 p.u.

With overlaps counted only once, the pairwise certification reduces the projected area by 19.1% relative to the unverified union of the original inner neighborhoods, while retaining a region substantially larger than any individual neighborhood and being comparable in extent to the normal voltage operating range. Operationally, the multi-center construction provides a single uniqueness certificate for a family of anticipated voltage-angle profiles, reducing the need for separate analyses as the operating point shifts within the composite region.

VIII. Conclusion and Future Directions

This paper develops a framework for characterizing HV regions with unique PF solutions. Exploiting the quadratic structure of the Cartesian-coordinate PF equations, we show that finding the largest centered hyperrectangle with a prescribed aspect ratio is exactly equivalent to solving a number of nonconvex QCQPs that grows linearly with the grid size. To our knowledge, this is the first exact characterization of such a PF uniqueness neighborhood. SDP and QC relaxations provide certified inner bounds, while feasible solutions obtained by an interior-point method provide outer bounds. We further develop a composition criterion that preserves injectivity over unions of neighborhoods, extending the guarantees to larger, potentially nonconvex regions. Tests on IEEE systems yield certified regions up to two orders of magnitude larger than existing alternatives and spanning voltage ranges representative of normal operation.

The main computational challenges are the scalability of the SDP-QC relaxations and the quadratic growth of pairwise Minkowski-average tests. Future directions include exploiting network sparsity and developing automated screening and composition methods to maximize certified coverage with fewer pairwise tests. Other extensions may consider extending the framework to more general load models and controllable transformer settings, and characterizing PF-input regions that guarantee the existence of a unique PF solution within the certified region.

ACKNOWLEDGMENT

The authors thank Enming Liang, Min Zhou, and Xiang Pan for their helpful discussions, and the anonymous reviewers for their constructive comments.

REFERENCES

[1] O. A. Afolabi, W. H. Ali, P. Cofie, J. Fuller, P. Obiomon, and E. S. Kolawole, "Analysis of the load flow problem in power system planning studies," *Energy and Power Engineering*, vol. 7, no. 10, pp. 509–523, 2015.

[2] A. Leite da Silva, S. Ribeiro, V. Arienti, R. Allan, and M. Do Coutto Filho, "Probabilistic load flow techniques applied to power system expansion planning," *IEEE Transactions on Power Systems*, vol. 5, no. 4, pp. 1047–1053, 1990.

[3] V. J. Mishra and M. D. Khardenvis, "Contingency analysis of power system," in *2012 IEEE Students' Conference on Electrical, Electronics and Computer Science*, 2012, pp. 1–4.

[4] M. Gholami, M. J. Sanjari, M. Safari, M. Akbari, and M. R. Kamali, "Static security assessment of power systems: A review," *International Transactions on Electrical Energy Systems*, vol. 30, no. 9, p. e12432, 2020.

[5] A. Klos and J. Wojcicka, "Physical aspects of the nonuniqueness of load flow solutions," *International Journal of Electrical Power & Energy Systems*, vol. 13, no. 5, pp. 268–276, 1991.

[6] C. Wang, A. Bernstein, J.-Y. Le Boudec, and M. Paolone, "Explicit conditions on existence and uniqueness of load-flow solutions in distribution networks," *IEEE Transactions on Smart Grid*, vol. 9, no. 2, pp. 953–962, 2018.

[7] C. Wang, A. Bernstein, J.-Y. Le, Boudec, and M. Paolone, "Existence and uniqueness of load-flow solutions in three-phase distribution networks," *IEEE Transactions on Power Systems*, vol. 32, no. 4, pp. 3319–3320, 2017.

[8] S. Bolognani and S. Zampieri, "On the existence and linear approximation of the power flow solution in power distribution networks," *IEEE Transactions on Power Systems*, vol. 31, no. 1, pp. 163–172, 2016.

[9] E. M. S. Duque, J. S. Giraldo, P. P. Vergara, P. H. Nguyen, and H. J. Slootweg, "Tensor power flow formulations for multidimensional analyses in distribution systems," *International Journal of Electrical Power & Energy Systems*, vol. 162, p. 110275, 2024.

[10] S. Park, R. Y. Zhang, J. Lavaei, and R. Baldick, "Uniqueness of power flow solutions using monotonicity and network topology," *IEEE Transactions on Control of Network Systems*, vol. 8, no. 1, pp. 319–330, 2021.

[11] H. Zhang, S. Park, J. Lavaei, and R. Baldick, "Uniqueness of power flow solutions using graph-theoretic notions," *IEEE Transactions on Control of Network Systems*, vol. 9, no. 1, pp. 100–112, 2022.

[12] P. Neupane and B. Cui, "A Cycle-Based Solvability Condition for Real Power Flow Equations," *IEEE Control Systems Letters*, vol. 10, pp. 1729–1734, 2026.

[13] K. Dvijotham, M. Chertkov, and S. Low, "A differential analysis of the power flow equations," in *2015 54th IEEE Conference on Decision and Control (CDC)*, Dec. 2015, pp. 23–30.

[14] K. Dvijotham, B. Krishnamoorthy, Y. Luo, and B. Rapone, "Robust feasibility of systems of quadratic equations using topological degree theory," *Optimization Letters*, vol. 18, no. 2, pp. 591–613, 2024.

[15] A. Jindal, D. Chatterjee, and R. Banavar, "Estimates of the size of the domain of the implicit function theorem: a mapping degree-based approach," *Mathematics of Control, Signals, and Systems*, vol. 36, no. 1, pp. 139–175, 2024.

[16] R. Abraham, J. E. Marsden, and T. Ratiu, *Manifolds, tensor analysis, and applications*. Springer Science & Business Media, 2012, vol. 75.

[17] K. Dvijotham, E. Mallada, and J. W. Simpson-Porco, "High-voltage solution in radial power networks: Existence, properties, and equivalent algorithms," *IEEE Control Systems Letters*, vol. 1, no. 2, pp. 322–327, 2017.

[18] D. K. Molzahn, B. C. Lesieutre, and C. L. DeMarco, "A sufficient condition for power flow insolvability with applications to voltage stability margins," *IEEE Transactions on Power Systems*, vol. 28, no. 3, pp. 2592–2601, 2013.

[19] D. Lee, H. D. Nguyen, K. Dvijotham, and K. Turitsyn, "Convex restriction of power flow feasibility sets," *IEEE Transactions on Control of Network Systems*, vol. 6, no. 3, pp. 1235–1245, 2019.

[20] B. Cui and X. A. Sun, "Securing voltage stability in power grids via holomorphic dynamics," *Automatica*, vol. 176, p. 112158, 2025.

[21] V. Ajjarapu and C. Christy, "The continuation power flow: a tool for steady state voltage stability analysis," *IEEE Transactions on Power Systems*, vol. 7, no. 1, pp. 416–423, 1992.

[22] R. C. Heitmann, "On the jacobian conjecture," *Journal of Pure and Applied Algebra*, vol. 64, no. 1, pp. 35–72, 1990.

[23] S. S.-S. Wang, "A jacobian criterion for separability," *Journal of Algebra*, vol. 65, no. 2, pp. 453–494, 1980.

[24] C. Pantea, H. Koeppl, and G. Craciun, "Global injectivity and multiple equilibria in uni- and bi-molecular reaction networks," *Discrete and Continuous Dynamical Systems - B*, vol. 17, no. 6, pp. 2153–2170, 2012.

[25] G. P. McCormick, "Computability of global solutions to factorable nonconvex programs: Part i—convex underestimating problems," *Mathematical programming*, vol. 10, pp. 147–175, 1976.

[26] M. Bynum, A. Castillo, J.-P. Watson, and C. D. Laird, "Strengthened socp relaxations for acopf with mccormick envelopes and bounds tightening," in *13th International Symposium on Process Systems Engineering (PSE 2018)*, ser. Computer Aided Chemical Engineering, M. R. Eden, M. G. Ierapetritou, and G. P. Towler, Eds. Elsevier, 2018, vol. 44, pp. 1555–1560.

[27] X. Bai, H. Wei, K. Fujisawa, and Y. Wang, "Semidefinite programming for optimal power flow problems," *International Journal of Electrical Power & Energy Systems*, vol. 30, no. 6, pp. 383–392, 2008.

[28] J. Lavaei and S. H. Low, "Zero duality gap in optimal power flow problem," *IEEE Transactions on Power Systems*, vol. 27, no. 1, pp. 92–107, 2012.

[29] H. Jiang, T. Kathuria, Y. T. Lee, S. Padmanabhan, and Z. Song, "A faster interior point method for semidefinite programming," in *2020 IEEE 61st Annual Symposium on Foundations of Computer Science (FOCS)*, 2020, pp. 910–918.

[30] F. A. Potra and S. J. Wright, "Interior-point methods," *Journal of Computational and Applied Mathematics*, vol. 124, no. 1, pp. 281–302, 2000.

[31] N. Dyn and E. Farkhi, "Spline subdivision schemes for compact sets: A survey," *Serdica Mathematical Journal*, vol. 28, no. 4, pp. 349–360, 2002.

[32] R. D. Zimmerman, C. E. Murillo-Sánchez, and R. J. Thomas, "Matpower: Steady-state operations, planning, and analysis tools for power systems research and education," *IEEE Transactions on power systems*, vol. 26, no. 1, pp. 12–19, 2010.

[33] G. Kron, *Tensor Analysis of Networks*. New York, NY, USA: Wiley, 1939.

[34] J. Löfberg, "Yalmip : A toolbox for modeling and optimization in matlab," in *Proc. CACSD Conference*, Taipei, Taiwan, 2004.

[35] M. ApS, *The MOSEK optimization toolbox for MATLAB manual. Version 9.0.*, 2019. [Online]. Available: http://docs.mosek.com/9.0/toolbox/index.html

[36] J. Currie and D. I. Wilson, "OPTI: Lowering the Barrier Between Open Source Optimizers and the Industrial MATLAB User," in *Proc. Foundations of Computer-Aided Process Operations*, Savannah, Georgia, USA, 2012.

[37] J. Wang, V. Magron, J. B. Lasserre, and N. H. A. Mai, "Cs-tssos: Correlative and term sparsity for large-scale polynomial optimization," *ACM Transactions on Mathematical Software*, vol. 48, no. 4, Dec. 2022.

[38] J. M. Aguirre, D. Cifuentes, V. Guigues, R. D. Monteiro, V. H. Nascimento, and A. Sujanani, "cuhallar: A gpu accelerated low-rank augmented lagrangian method for large-scale semidefinite programming," *arXiv preprint arXiv:2505.13719*, 2025.

[39] D. K. Molzahn, J. T. Holzer, B. C. Lesieutre, and C. L. DeMarco, "Implementation of a large-scale optimal power flow solver based on semidefinite programming," *IEEE Transactions on Power Systems*, vol. 28, no. 4, pp. 3987–3998, 2013.

APPENDIX A
PROOF OF PROPOSITION 1

A. Proof of Part (1): $0 < r^*(\mathbf{v}_0, \kappa) < \infty$

Proof. Since $J_g(\mathbf{v}_0)$ is nonsingular, the inverse function theorem [16] guarantees an open neighborhood $\hat{B}_v$ of $\mathbf{v}_0$ on which g is invertible and hence injective. Because $\hat{B}_v$ is open, for any fixed $\kappa > 0$ there exists $r_0 > 0$ such that $B(\mathbf{v}_0, \kappa, r_0) \subseteq \hat{B}_v$. Therefore, g is injective on $B(\mathbf{v}_0, \kappa, r_0)$ and, by the definition of r^*, $r^*(\mathbf{v}_0, \kappa) \geq r_0 > 0$.

To show $r^*(\mathbf{v}_0,\kappa) < \infty$, assume for contradiction that $r^*(\mathbf{v}_0,\kappa) = \infty$. We use the following midpoint identity for the quadratic mapping g: for any $\mathbf{v}_1, \mathbf{v}_2 \in B(\mathbf{v}_0,\kappa,r)$,

$$g(\mathbf{v}_1) - g(\mathbf{v}_2) = J_g\left(\frac{\mathbf{v}_1+\mathbf{v}_2}{2}\right)(\mathbf{v}_1-\mathbf{v}_2). \tag{13}$$

By assumption, $J_g(\mathbf{v})$ is singular at some $\mathbf{v} \in \mathbb{R}^{2(N-1)}$, so there exists $\mathbf{d} \neq \mathbf{0}$ such that $J_g(\mathbf{v})\mathbf{d} = \mathbf{0}$. Choose r sufficiently large that $\mathbf{v} \in B(\mathbf{v}_0,\kappa,r)$. By openness, $\mathbf{v} \pm \epsilon\mathbf{d}$ also belong to this neighborhood for sufficiently small $\epsilon > 0$. The formulation (13) then gives $g(\mathbf{v}+\epsilon\mathbf{d}) = g(\mathbf{v}-\epsilon\mathbf{d})$, contradicting injectivity. Hence, $r^*(\mathbf{v}_0,\kappa) < \infty$. □

B. Proof of Parts (2) and (3): Monotonicity Properties

Proof. Let $0 < \kappa_1 < \kappa_2$. Because each neighborhood is maximum for its prescribed aspect ratio, neither neighborhood can have both a strictly larger real-voltage half-width and a strictly larger imaginary-voltage half-width than the other. Otherwise, the maximality of the contained neighborhood would be contradicted.

- *Non-Increasing* r^*: Suppose for contradiction that $r^*(\mathbf{v}_0,\kappa_1) < r^*(\mathbf{v}_0,\kappa_2)$. Then, $\kappa_1 \cdot r^*(\mathbf{v}_0,\kappa_1) < \kappa_2 \cdot r^*(\mathbf{v}_0,\kappa_2)$ (since $\kappa_1 < \kappa_2$), and $B(\mathbf{v}_0,\kappa_1,r^*(\mathbf{v}_0,\kappa_1))$ would be contained within $B(\mathbf{v}_0,\kappa_2,r^*(\mathbf{v}_0,\kappa_2))$, contradicting non-inclusion and optimality. Thus, $r^*(\mathbf{v}_0,\kappa)$ is non-increasing.
- *Non-Decreasing* κr^*: Suppose for contradiction that $\kappa_1 \cdot r^*(\mathbf{v}_0,\kappa_1) > \kappa_2 \cdot r^*(\mathbf{v}_0,\kappa_2)$. Then, $r^*(\mathbf{v}_0,\kappa_1) > r^*(\mathbf{v}_0,\kappa_2)$ (since $\kappa_1 < \kappa_2$), and $B(\mathbf{v}_0,\kappa_2,r^*(\mathbf{v}_0,\kappa_2))$ would be contained within $B(\mathbf{v}_0,\kappa_1,r^*(\mathbf{v}_0,\kappa_1))$, contradicting non-inclusion and optimality. Thus, $\kappa \cdot r^*(\mathbf{v}_0,\kappa)$ is non-decreasing.

(Note: Monotonicity may not be strict if no new singularities are introduced for certain κ changes.) □

APPENDIX B
PROOF OF THEOREM 1

Proof. We aim to prove that the given pairwise Jacobian nonsingularity condition ensures injectivity of g over the union $\bigcup_{i=1}^m B_i$. Suppose, for contradiction, that there exist distinct $\mathbf{v}_1, \mathbf{v}_2 \in \bigcup_{i=1}^m B_i$ such that $g(\mathbf{v}_1) = g(\mathbf{v}_2)$. If both points belong to the same B_i, this contradicts the assumed injectivity of g on B_i. Otherwise, choose $i \neq j$ such that $\mathbf{v}_1 \in B_i$ and $\mathbf{v}_2 \in B_j$. Applying the midpoint identity above and using $g(\mathbf{v}_1) = g(\mathbf{v}_2)$ gives

$$\mathbf{0} = g(\mathbf{v}_1) - g(\mathbf{v}_2) = J_g\left(\frac{\mathbf{v}_1+\mathbf{v}_2}{2}\right)(\mathbf{v}_1-\mathbf{v}_2).$$

Since $\mathbf{v}_1 - \mathbf{v}_2 \neq \mathbf{0}$, the Jacobian at the midpoint is singular. However, $(\mathbf{v}_1+\mathbf{v}_2)/2 \in (B_i + B_j)/2$, where the theorem assumes J_g is nonsingular over the entire region $(B_i+B_j)/2$. This contradiction establishes that g is injective on $\bigcup_{i=1}^m B_i$. □

APPENDIX C
CONVEX ENVELOPE FOR BILINEAR TERMS

For a bilinear equality $t = xy$ over the fixed bounds $x_L \le x \le x_U$ and $y_L \le y \le y_U$, its McCormick envelope [25] is described by

$$\begin{aligned} &t \ge x_L y + x y_L - x_L y_L, \qquad &&t \ge x_U y + x y_U - x_U y_U, \\ &t \le x_U y + x y_L - x_U y_L, \qquad &&t \le x_L y + x y_U - x_L y_U. \end{aligned}$$

In the SDP-QC relaxation, these inequalities are applied to the products $e_i z_j$ and $f_i z_j$, where $i = 1, ..., N-1$ and $j = 1, ..., 2(N-1)$. For $\mathbf{v}_0 = [\mathbf{e}_0^\top, \mathbf{f}_0^\top]^\top$, the relevant bounds are $e_i \in [e_{0,i} - r_t, e_{0,i} + r_t]$, $f_i \in [f_{0,i} - \kappa r_t, f_{0,i} + \kappa r_t]$, and $z_j \in [-1, 1]$, where $r_t \ge 0$. Substitution into the McCormick inequalities yields

$$\begin{cases} e_i z_j \ge (e_{0,i} - r_t) z_j - e_i + e_{0,i} - r_t, \\ e_i z_j \ge (e_{0,i} + r_t) z_j + e_i - e_{0,i} - r_t, \\ e_i z_j \le (e_{0,i} + r_t) z_j - e_i + e_{0,i} + r_t, \\ e_i z_j \le (e_{0,i} - r_t) z_j + e_i - e_{0,i} + r_t, \end{cases}$$

$$\begin{cases} f_i z_j \ge (f_{0,i} - \kappa r_t) z_j - f_i + f_{0,i} - \kappa r_t, \\ f_i z_j \ge (f_{0,i} + \kappa r_t) z_j + f_i - f_{0,i} - \kappa r_t, \\ f_i z_j \le (f_{0,i} + \kappa r_t) z_j - f_i + f_{0,i} + \kappa r_t, \\ f_i z_j \le (f_{0,i} - \kappa r_t) z_j + f_i - f_{0,i} + \kappa r_t. \end{cases}$$

Because the voltage bounds depend on the decision variable r_t, the resulting inequalities contain the additional products $r_t z_j$. In the lifted formulation, the products $e_i z_j$, $f_i z_j$, and $r_t z_j$ are replaced by $W_{(i)(j+2N)}$, $W_{(i+N)(j+2N)}$, and $W_{(N_x)(j+2N)}$, respectively. Moreover, since the fixed slack-bus component satisfies $e_N = 1$, each linear variable can be written as a bilinear product. For example, $e_i = e_N e_i$, which is represented by $W_{(N)(i)}$ in the lifted formulation.

APPENDIX D
DERIVATION OF THE SCALING FACTOR IN THE HV-NEIGHBORHOOD COMPOSITION PROCEDURE

We derive the optimal common scaling factor used when $r_{ij}^* < \bar{r}_{ij}$, where the pairwise Minkowski-average parameters r_{ij}^* and $\bar{r}_{ij}$ are defined in Section VI. Let

$$\widehat{B}_i = B(\mathbf{v}_{0i}, \kappa_i, r_i'), \qquad \widehat{B}_j = B(\mathbf{v}_{0j}, \kappa_j, r_j')$$

denote the adjusted neighborhoods. We restrict the adjustment to a common scaling factor,

$$\tau = \frac{r_i'}{r_i} = \frac{r_j'}{r_j},$$

which preserves the relative sizes of the two neighborhoods and the aspect ratio $\bar{\kappa}_{ij}$ of their Minkowski average.

To retain neighborhoods that are as large as possible under this common-shrinking strategy while ensuring Jacobian nonsingularity throughout their Minkowski average, we maximize the sum of their projected areas:

$$\begin{aligned} \max \quad & \kappa_i (r_i')^2 + \kappa_j (r_j')^2 \\ \text{s.t.} \quad & \frac{r_i' + r_j'}{2} \le r^*(\bar{\mathbf{v}}_{0ij}, \bar{\kappa}_{ij}), \\ & r_i' = \tau r_i, \quad r_j' = \tau r_j, \\ & 0 < \tau \le 1, \\ \text{var.} \quad & r_i', r_j', \tau. \end{aligned} \tag{14}$$

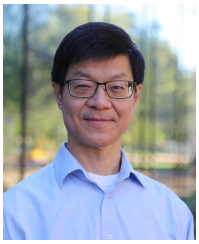
The optimal solution scales the original neighborhoods by a scaling factor $\tau = r^*(\bar{\mathbf{v}}_{0ij}, \bar{\kappa}_{ij})/\bar{r}_{ij}$, yielding $r_i' = \tau \cdot r_i$ and $r_j' = \tau \cdot r_j$. Since $r^*(\bar{\mathbf{v}}_{0ij}, \bar{\kappa}_{ij}) < \bar{r}_{ij}$, we have $\tau \in (0, 1)$. Thus, τ is the largest common scaling factor that ensures Jacobian nonsingularity throughout the adjusted Minkowski-average set.



Jiawei Zhao received the B.Eng. degree in Electrical Engineering and Automation from Zhejiang University, Hangzhou, China, in 2021, and the M.Sc. degree in Data-Driven Modeling from The Hong Kong University of Science and Technology, Hong Kong, in 2022. She is currently pursuing the Ph.D. degree with the Department of Data Science, City University of Hong Kong, Hong Kong. Her research interests include machine learning and its applications to power system analysis, as well as the theoretical foundations of power flow analysis.



Minghua Chen (S'04 M'06 SM' 13 F'22) received his B.Eng. and M.S. degrees from the Department of Electronic Engineering at Tsinghua University. He received his Ph.D. degree from the Department of Electrical Engineering and Computer Sciences at University of California Berkeley. He is currently a Presidential Chair Professor at School of Data Science, The Chinese University of Hong Kong, Shenzhen. He is on leave with Department of Data Science, City University of Hong Kong. Minghua received the Eli Jury award from UC Berkeley in 2007 (presented to a graduate student or recent alumnus for outstanding achievement in the area of Systems, Communications, Control, or Signal Processing) and The Chinese University of Hong Kong Young Researcher Award in 2013. He also received IEEE ICME Best Paper Award in 2009, IEEE Transactions on Multimedia Prize Paper Award in 2009, ACM Multimedia Best Paper Award in 2012, IEEE INFOCOM Best Poster Award in 2021, ACM e-Energy Best Paper Award in 2023, Gradient AI Research Award in 2024, and Nature Communications Editors' Highlights in 2025. He receives the ACM Recognition of Service Award in 2017 and 2020 for the service contribution to the research community. He is currently an Area/Track Chair of IEEE INFOCOM, ACM e-Energy, NeurIPS, and ICML, and Award Chair of ACM SIGEnergy. Minghua's recent research interests include online optimization and algorithms, machine learning and its applications in power system operation, intelligent transportation systems, distributed optimization, and delay-critical networked systems. He is a Fellow of the IEEE.



Steven Low is the Gilloon Professor of the Computing & Mathematical Sciences Department and the Electrical Engineering Department at Caltech. Before that, he was with AT&T Bell Laboratories, Murray Hill, NJ, and the University of Melbourne, Australia. He was an awardee of the IEEE Koji Kobayashi Computers and Communications Award, the IEEE INFOCOM Achievement Award, the ACM SIGEnergy Achievement Award, and the ACM SIGMetrics Test of Time Award. He is a Fellow of IEEE, ACM, and CSEE. He is known for research on Internet congestion control and optimal power flow problems in smart grid. His research has been deployed in practice for content distribution and for electric vehicle charging. His text Power System Analysis: Analytical Tools and Structural Properties will be published by Cambridge. He received his B.S. from Cornell and PhD from Berkeley, both in EE.